

Fabrication and dielectric properties of $\text{Ba}_{0.6}\text{Sr}_{0.4}\text{TiO}_3$ / acrylonitrile–butadiene–styrene resin composites

Kena Zhang¹ · Feng Gao¹ · Jie Xu¹ · Li Wang¹ · Qingqing Zhang¹ · Jie Kong²

Received: 24 January 2017 / Accepted: 18 February 2017 / Published online: 1 March 2017
© Springer Science+Business Media New York 2017

Abstract $\text{Ba}_{0.6}\text{Sr}_{0.4}\text{TiO}_3$ (BST)/acrylonitrile–butadiene–styrene (ABS) composites were prepared via solution casting method. Effects of volume fraction of BST on microstructure and dielectric properties of composites were studied. Dielectric constants were simulated by Lichtenecker, Maxwell, Landzu–Lifshitz, and Yamada models. It was found that the permittivity of BST/ABS resin composites increases from 4.5 to 18 while loss tangent from 0.021 to 0.082 at 1 kHz with BST fillers increasing from 10 to 40 vol%. The permittivity value calculated by Yamada’s model matched well with the experimental results and the deviation was less than 2% with a shape factor (n) of 3.2. The dielectric tunability of the composites improved with increasing the amount of BST fillers. Dielectric properties of ABS resins were enhanced by increasing BST fillers due to the interface polarization mechanism. The development of BST/ABS dielectric functional composites broadens the range of candidate materials for 3D printed electronic devices.

1 Introduction

The $(\text{BaSr})\text{TiO}_3$ ceramics, a intensively investigated ferroelectric, have received lots of attentions due to their unique properties including high permittivity and tunability [1, 2]. They are considered as promising candidates in a wide range of electronic applications, such as microwave phase shifters, tunable phased-array antenna and varactors [3–5]. In fact, the dielectric ceramics possess excellent dielectric properties. However, they also have some drawbacks like poor flexibility which is not satisfied with the fabrication of electric devices. On the other hand, from the application point of view, in order to meet the impedance matching [6, 7] the dielectric properties for tunable devices should have relatively low permittivity and high tunability. Nevertheless, the reality is not so optimistic that the dielectrics with high tunability usually possess high permittivity [8]. Thus, several methods have been applied for the sake of reducing the permittivity of dielectrics including ion doping, solid solution, and air bubbles, etc [9, 10]. Among others, a strategy to obtain composites by combining polymers with ceramic fillers has been developed to solve this problem [11–18], which may follow up with the application of microwave tunable devices and possess the benefits of appropriate dielectric constant, easy fabrication as well as relatively low dielectric loss [19, 20].

In recent years, 3D printing has received broad interest because of its high efficient, low cost and potential of fabricating complex devices in a single direct process from computer design and control. However, dielectric functional devices that might be obtained by 3D printing are restricted due to the limitation of current dielectric materials made by the 3D printing process [21, 22]. Acrylonitrile–butadiene–styrene (ABS) resin (copolymer of styrene, acrylonitrile and butadiene), one of the widely 3D printing used

✉ Feng Gao
gaofeng@nwpu.edu.cn

¹ State Key Laboratory of Solidification Processing, MIIT Key Laboratory of Radiation Detection Materials and Devices, School of Materials Science and Engineering, Northwestern Polytechnical University, Xi’an 710072, People’s Republic of China

² Shaanxi Key Laboratory of Macromolecular Science and Technology, School of Science, Northwestern Polytechnical University, Xi’an 710072, People’s Republic of China

materials with low dielectric constant (~ 4.5), dielectric loss (~ 0.045) and excellent dielectric strength (~ 206 kV/mm), is an important interchangeable thermo-plasticity engineering plastic in which nitrile and phenyl group will provide compatibility while unsaturated double bond will give the copolymer good mechanical flexibility. In addition, their properties can be tuned to meet the requirement by changing the proportions of constituents. Hence, ABS copolymer can be used as the polymer matrix of ceramic/polymer functional dielectric composites which could be applied to 3D printing. Considering above all, composites combined the advantages of $(\text{BaSr})\text{TiO}_3$ ceramics and ABS copolymer while eliminating the drawbacks are expected to be a desirable material for 3D printed microwave tunable device which also has scarcely been studied.

In this paper, $\text{Ba}_{0.6}\text{Sr}_{0.4}\text{TiO}_3$ (BST) ceramic powders were obtained by conventional solid state reaction and the surface of these powders was modified by H_2O_2 to introduce plenty of hydroxyl groups that can ameliorate the interface contact between polymer and ceramics [23, 24]. BST/ABS composites were fabricated by tape casting and hot pressing method. The microstructure, thermal and dielectric properties of these composites as a function of ceramic concentration were investigated and the interfacial connection mechanism was discussed. Various dielectric theoretical models, such as Lichtenecker, Maxwell–Garnett, Landzu–Lifshitz and Yamada model were employed to analyze and simulate the dielectric constant.

2 Experimental procedure

2.1 Preparation of BST/ABS resin composites

In this work, BST/ABS resin composites were obtained from $\text{Ba}_{0.6}\text{Sr}_{0.4}\text{TiO}_3$ (BST) ceramic powders and ABS copolymer based on the general formula $\text{ABS} + x\text{BST}$, where x is 10, 20, 30, and 40 vol%, respectively. The micron-size $\text{Ba}_{0.6}\text{Sr}_{0.4}\text{TiO}_3$ with amorphous morphology powders were prepared by traditional solid state reaction with a stoichiometric mixing of BaCO_3 , SrCO_3 , and TiO_2 which were heating at 1400°C for 2 h accompanying repeated grinding [8]. The BST powders were dispersed in an aqueous solution of H_2O_2 (30%, 500 mL) by a magnetic stirring at 80°C for 2 h, and then modified BST powders were obtained after vacuum drying at 60°C for 10 h. The resulting BST particles had an amorphous microstructure [23].

The ABS matrix was commercial product supplied by Zhuhai Three Green Industrial Co., Ltd., and *N,N*-dimethylformamide (DMF, anhydrous 99.8%) was picked up from Sinopharm Chemical Reagent Co., Ltd. The modified BST powders and ABS particles were dispersed in DMF

under magnetic stirring for 2 h at 50°C and ultra-sonicated for 1 h to obtain an uniform suspension. Then the slurry was achieved by mechanical milling the mixed solution at 600 rpm for 12 h. The BST/ABS composite thick film was subsequently made by casting the mixture on a glass substrate. After that, the film was kept in a vacuum oven overnight at 60°C to evaporate the organic solvent of DMF. Then the BST/ABS films with $0.02\sim 0.2$ mm in thickness were produced by hot pressed at 150°C for 2 h. The surface of the specimen was coated by silver paste as the electrode to fulfil dielectric measurements.

2.2 Characterization

The microstructure and morphology of composites were observed by scanning electron microscopy (SEM, TESCAN VEGA3). To measure the thermal properties of BST/ABS films at the temperature range from 20 to 800°C and at a heating rate of $10^\circ\text{C}/\text{min}$ in flowing N_2 atmosphere (flow rate: 50 mL/min), the TA Instruments (USA model: TA-SDT2960) with alumina as the reference material were employed. In addition, the dielectric properties were analyzed using a high-precision impedance analyzer (WK P6505). The relative tunability of the composites was measured at 1 kHz with a bias voltage source.

3 Results and discussion

3.1 Microstructure of BST/ABS composites

Figure 1 shows the cross section morphology images of the BST/ABS resin composites with 10, 20, 30 and 40 vol% volume concentration of ceramic phase, respectively. It can be observed that BST particles are included and well-dispersed in ABS matrix without evident agglomeration and quantity of porosity due to the molecule interaction between BST and ABS. Thus, it demonstrates that uniform BST/ABS composites can be formed by solution casting method. In addition, the increasing content of BST ceramic fillers can break down the ABS macro-continuity that can be replaced by hydrogen bonds between the $-\text{CN}$ group of ABS molecular chains and the $-\text{OH}$ group on the surface of ceramic particles [25, 26].

The schematic mechanism of the hydroxylation of BST particles and hydrogen bonding reaction between BST and ABS is shown in Fig. 2. Large quantity of hydroxyl groups is adhered to the BST surface by reacting with H_2O_2 due to the hydrophilicity of BST particles. Hydrogen bonds generate from the $-\text{CN}$ and $-\text{OH}$ groups through ball-mill mixing so as to produce a strong interface interaction between BST fillers and ABS matrix and the former becomes uniformly dispersed in the latter as a consequence.

Fig. 1 SEM images of the BST/ABS composites with different BST contents: **a** 10 vol%; **b** 20 vol%; **c** 30 vol%; **d** 40 vol%

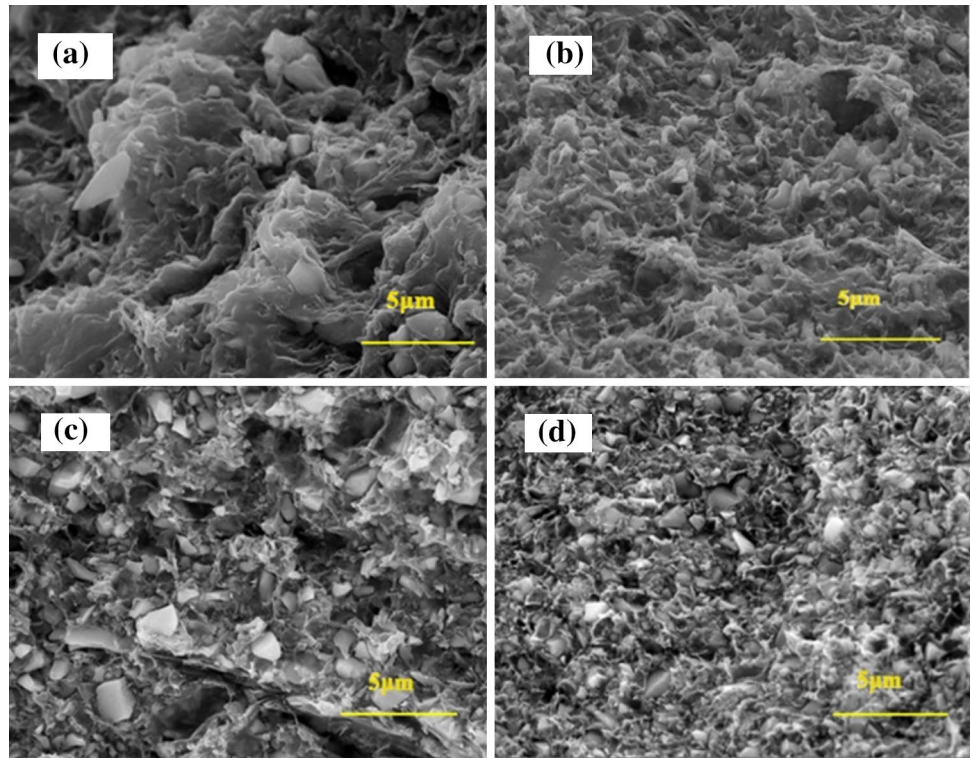
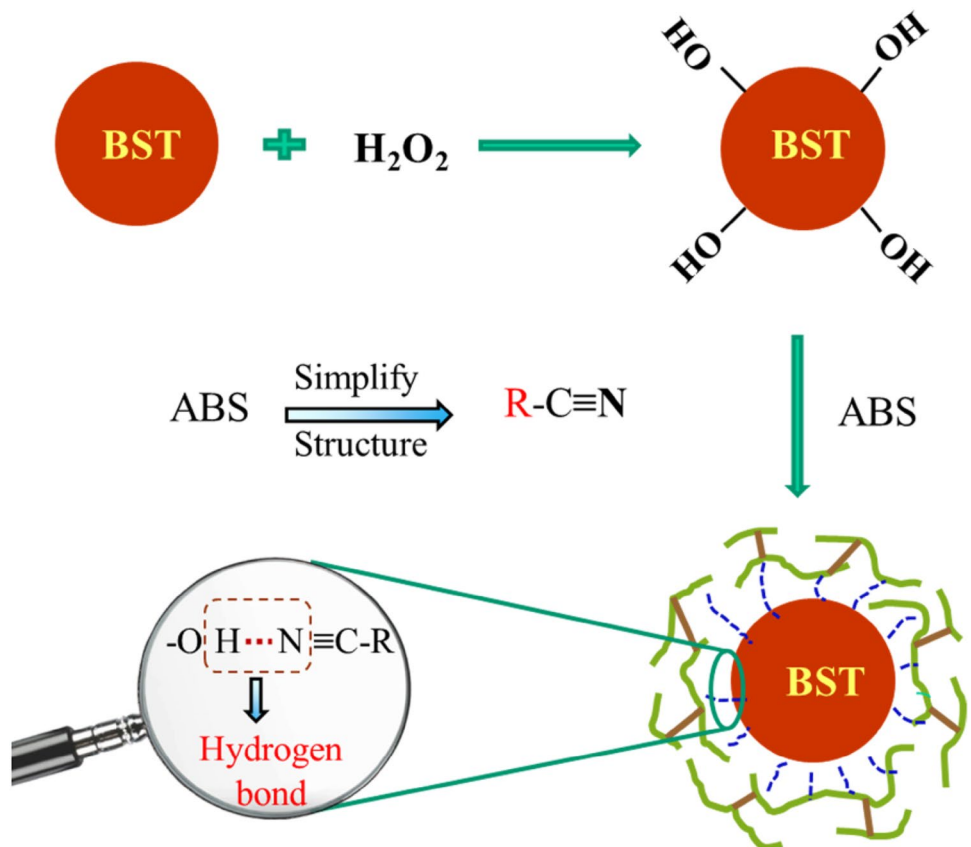


Fig. 2 Forming mechanism of the BST/ABS composites



3.2 Thermal properties of BST/ABS composites

Figure 3 shows thermal analysis curves of pure BST or ABS and BST/ABS composites that were measured by using TGA and DSC, respectively. It can be seen from Fig. 3a that pure ABS and BST/ABS composites exhibit a little total mass loss at around 150~200°C. The mass loss is mainly due to the evaporation of DMF solvents hidden within materials and water molecules absorbed on the surface of materials. Secondly, it can be observed that pure ABS and BST/ABS composites experience a drastic weight loss at the range of 350~500°C that are attributed to the decomposition of organic matter while the pure BST ceramic powders do not, which indicates remarkable temperature stability. Moreover, the endothermic peak in the range of 100~150°C originates from the transformation of their glassy state into switched from their glassy into elastomeric state of the ABS organic matrix that is an endothermic physical reaction, as shown in Fig. 3b. In addition, it is well known that ABS is composed by the

acrylonitrile-styrene copolymer as continuous matrix phase and the polybutadiene particles as dispersed phase. Hence, the presence of two exothermic peaks around 350~500°C are produced by thermal degradation of the two parts of ABS matrix, which is in correspondence to the result of TGA measurement. It can also be concluded that the decrease of weight loss and exothermic peaks of composites are attributed to the addition of BST fillers which can improve the thermal stability of the composites.

3.3 Dielectric properties of BST/ABS composites

The frequency dependence of the dielectric constant of the composites with BST volume fraction at 0, 10, 20, 30 and 40 vol% are shown in Fig. 4a. It can be found that there is an increase of dielectric constant from 4.5 to 18 (at 1 kHz) with increasing the volume fraction (i.e., 10–40 vol%) of BST, since the BST particles possess relatively high dielectric constant. The mechanism of this phenomenon can be explained by the interfacial polarization occurring in the

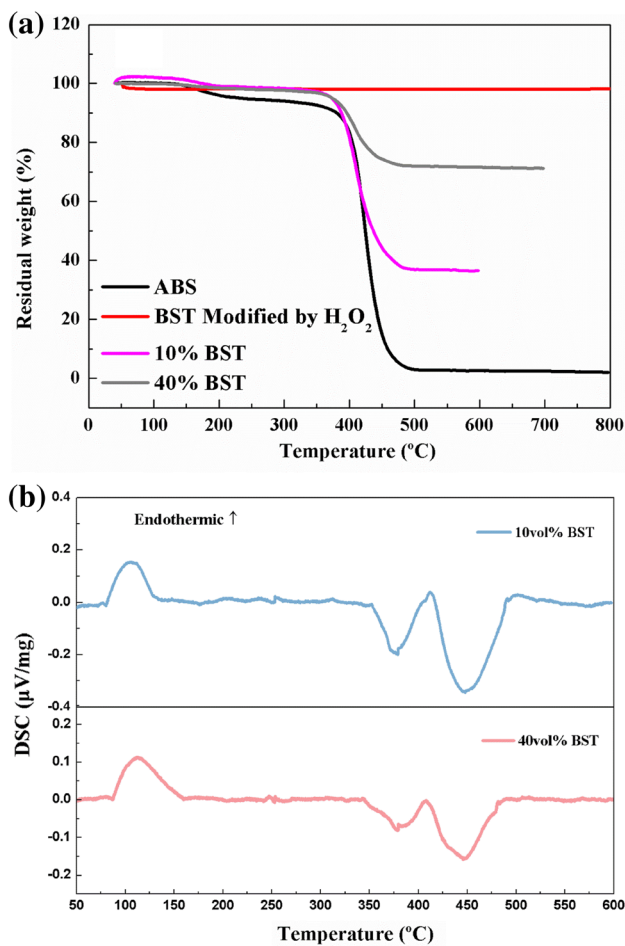


Fig. 3 The thermal analysis of ABS, BST and BST/ABS composites: **a** TGA; **b** DSC

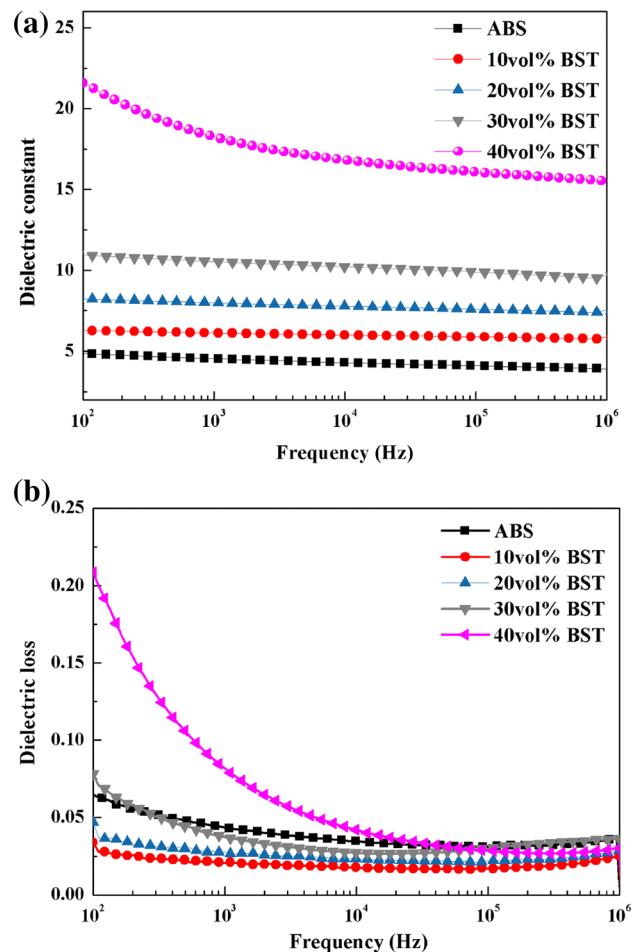


Fig. 4 Frequency dependence of dielectric properties of BST/ABS composites: **a** Dielectric constant; **b** Dielectric loss

inner microstructure of the BST/ABS composites which is shown in Fig. 5. There are lots of defects at the interface location between BST and ABS. There is no doubt that carriers like electron, hole and ion vacancy, etc. are assembled easily toward the defects. These restrained carriers migrate difficultly and distribute randomly without applied electric field, as shown in Fig. 5a. Then, the interfacial polarization is caused by the produced and ordered electric dipole moments with applied electric field, as shown in Fig. 5b. As a result, the interfacial polarization reaction increases and contributes to higher dielectric constant of composites with the ceramic loading volume increase. On the other hand, the dielectric constant of all the composites decreases with increasing frequency, which could be due to the polarization relaxation happened in the microstructure of composites, including interface polarization and dipole orientation polarization. Under the condition of low frequency, all polarization mechanisms mentioned above can respond timely on the change of frequency, while the interfacial polarization of composites does not under relatively high frequency. Consequently, the decrease of dielectric constant is thought to be responsible for weakening of the dipole orientation resulted from the increase of frequency.

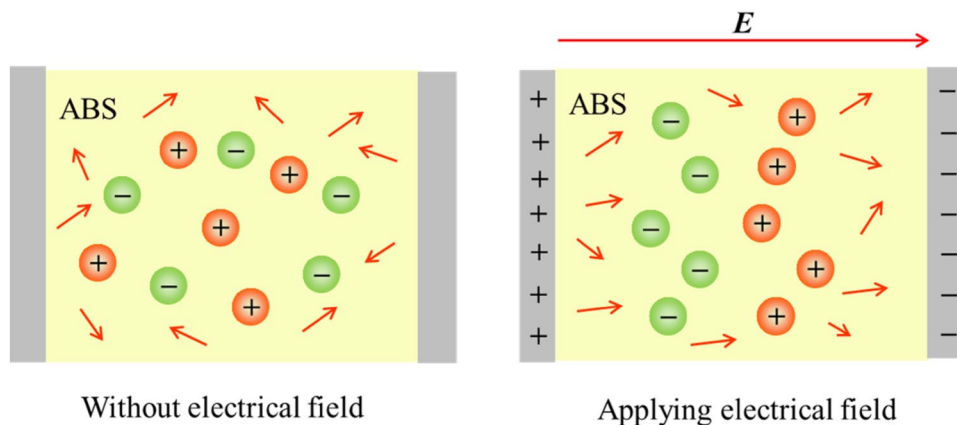
Dependence of dielectric loss of composites on frequency in the range of $10^2 \sim 10^6$ Hz at room temperature is shown in Fig. 4b. The result of dielectric loss is analyzed for the change trend which can be expounded that the loss decreases at low frequency range ($10^2 \sim 10^5$ Hz) while gradually move higher, besides, the pure ABS shows higher dielectric loss than others at comparatively high frequency. The conductive loss originated from the interfacial polarization strongly affects the dielectric loss at low frequency. The results demonstrate that dielectric loss increases from 0.021 to 0.082 at 1 kHz due to the increased interaction strength of interfacial polarization as the ceramic fillers volume increases. As frequency increases, there is a down trending in dielectric loss data. The reason is that the interfacial polarization fails to follow the electric field change

and hasn't contributed to dielectric loss of composites. On the other hand, the slightly increasing dielectric loss depends heavily on a Debye relaxation behavior at high frequency that stems from the $-\text{CH}$ and $-\text{CN}$ dipoles orientation polarization of the ABS matrix [27]. That is because the response time of dipoles orientation polarization is slightly slower than electric field change and the former lags behind the latter.

The temperature dependence of dielectric constant on temperature for composites at 1 kHz is given in Fig. 6a. It is found that the dielectric constant increases with temperature increasing from $25 \sim 120^\circ\text{C}$ due to the lifting dipole orientation polarization level. In the low temperature range, relatively low dielectric constant is related to freezing dipoles in the amorphous region that cannot move with the change of applied electric field, causing the obstruction of the relaxation polarization. An increasing dielectric constant in the range of $70 \sim 120^\circ\text{C}$ is ascribed to the decreasing relaxation time that can keep up with the change of applied electric field. One reason is that the dipoles attached to the polymer chain that accompanied with enough thermal energy can rotate quickly. Another important cause is that the thermal expansion of ceramic crystal produced gradually with the rising of temperature resulting in the movement of domains located in the single large grains, which can also lead to the increasing dielectric constant [28].

Figure 6b shows the temperature dependence of loss tangent of BST/ABS composites at 1 kHz. The loss increases dramatically with increasing temperature from room temperature to T_g and then decreasing after reaching a maximum at temperatures of $70 \sim 120^\circ\text{C}$. The change trend of dielectric loss is consistent with the dielectric constant. Again, the dielectric loss peak is broadened and flattened with increasing amount of BST fillers in ABS matrix. These phase transitions occur over a wide range of temperature when the BST content increases. This dispersion of phase transitions is a typical dielectric relaxation that stems from

Fig. 5 Model of interfacial polarization in the BST/ABS composites



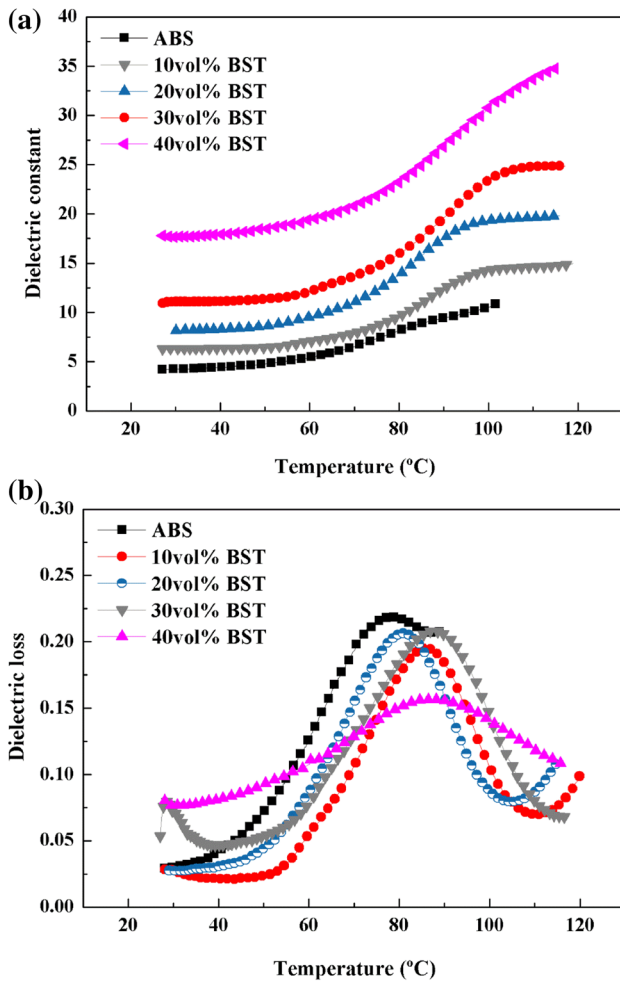


Fig. 6 Temperature dependence of dielectric properties of BST/ABS composites: **a** Dielectric constant; **b** Dielectric loss

two factors. One factor is the Debye relaxation behavior which is associated with the rotation and orientation of the –CN groups of the polymer matrix under applied electric field. The other is attributed to the interface polarization occurring in the heterogeneous interface between BST fillers and ABS polymers.

In order to measure a non-linear change that occurs in the dielectric permittivity and the applied electric field, the dielectric tunability (*T*) of the material is determined from Eq. (1):

$$T = \frac{\epsilon_{(0)} - \epsilon_{(E)}}{\epsilon_{(0)}} \times 100\% \tag{1}$$

where $\epsilon_{(0)}$ and $\epsilon_{(E)}$ are the dielectric permittivity under zero direct current (dc) electric field and under some given electric field, respectively. In this work, $E = 1.0$ and 2.0 kV/mm are applied as the criterion for comparing the tunability of composites and the results are shown in the Fig. 7. It is clear that the dielectric tunability of BST/ABS composites

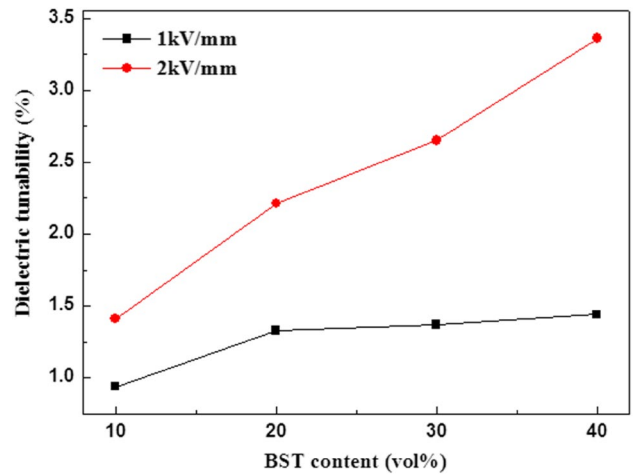


Fig. 7 The dielectric tunability of BST/ABS composites

increases as the BST loading volume increases at 1 kHz. In particular, the dielectric tunability of BST/ABS composites reached 1.41, 2.21, 2.65 and 3.36% with different BST filler contents (under the bias voltage 2.0 kV/mm). It is known that ABS polymer possesses the characteristic of low dielectric constant and no dielectric tunability measured experimentally. As a result, BST can improve the dielectric tunability properties of ABS polymer matrix.

3.4 Theoretical simulation for the dielectric constant of BST/ABS composites

Several kinds of models were used to predict the dielectric constant of the composites which could reduce the uncertainty of preparation process and improve the efficiency of research and development. Lichtenecker model [29] is a fundamental analytical model characterized by the logarithmic mixture rule. The rule can be expressed as follows:

$$\log \epsilon_r = \delta_c \log \epsilon_c + \delta_p \log \epsilon_p \tag{2}$$

where ϵ_c , ϵ_p , δ_c and δ_p are the dielectric constants of BST and ABS, the volume fraction of BST and ABS, respectively. However, this relation is only appropriate to forecast the dielectric constant of composites with similar value of dielectric constant of two constituent phases. Thus, the modified formula called Landzu-Lisfshitz’s model is shown as follows [30].

$$\epsilon_r = \epsilon_p \left[1 + 3\delta_c \left(\frac{\epsilon_c - \epsilon_p}{\epsilon_c + 2\epsilon_p} \right) \right] \tag{3}$$

This formula is more applicable to the composites with great difference dielectric constant between fillers

and matrix. Maxwell–Garnett model is also used to predict the dielectric constant of composites [31], which is formed by dispersing fillers homogeneously into matrix.

$$\epsilon_r = 1 + \frac{3\delta_c(\epsilon_c - \epsilon_p)}{\delta_p(\epsilon_c - \epsilon_p) + 3\epsilon_p} \quad (4)$$

While this model does not take into account the conductivity and spherical shape of the filler particles, which lead to produce error between experimental values and calculated results.

Yamada [32] proposed a new model where the shape factor of ceramic fillers was adequately considered. The dielectric constant of composites can be obtained from the following equation:

$$\epsilon_r = \epsilon_p \left[1 + \frac{n\delta_c(\epsilon_c - \epsilon_p)}{n\epsilon_p + \delta_p(\epsilon_c - \epsilon_p)} \right] \quad (5)$$

where “ n ” is the geometry-dependent parameter of the ceramic particles. The decrease inaccuracy of simulated and experimental values by adjusting the value of “ n ” is benefit to predict precisely the dielectric constant.

According to Eq. (5), the values of dielectric constant could be calculated by substituting the ϵ_c and ϵ_p with 3800 and 4.5 (at 1 kHz). Figure 8 shows the results with different shape factors (n) and volume fractions of ceramic fillers (δ_c); the values of δ_c are 0.1, 0.2, 0.3, 0.4 and n values are 0.5, 1, 3, 3.2, 3.5, respectively. As the figure illustrates, the simulation value increases with increasing δ_c and n . The results show that the simulation values using $n=3.2$ and $\delta_c < 0.4$ are consistent with the experiment data and the maximum error is less than 2%. Based on the above, one can draw a point that $n=3.2$ corresponds to micron-size BST particles with amorphous morphology. Therefore,

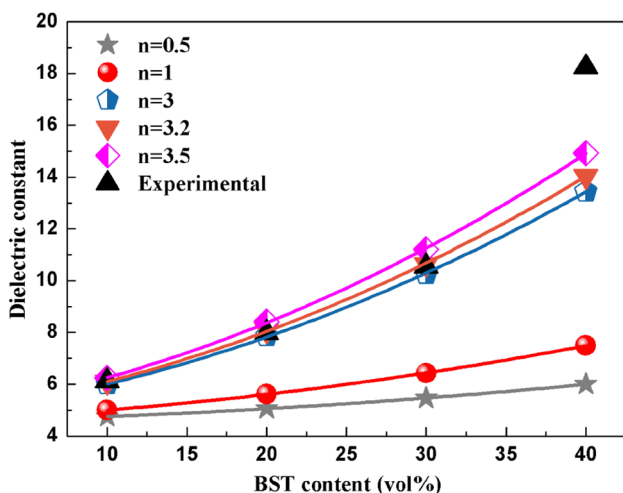


Fig. 8 The variation of dielectric constant of BST/ABS composites with shape factor and volume fraction of BST ceramics

the dielectric constant and its changing rule with different ceramics shape can be accurately simulated by adjusting n parameter.

The theoretical predictions values (TV) and experimental values (EV) of BST/ABS composites in terms of frequency with different volume fractions of BST are shown in Fig. 9. It is observed that the Yamada model has a good reliability to predict the dielectric constant of composites as the experimental values have a little error to the theory values when the content of ceramics is less than 40 vol%. On the contrary, the deviation of TV and EV enlarges when ceramic content approach to 40 vol%. This is assumed that more considering defects are generating and they can capture the carrier charge with increasing the ceramic content. As a result, the strengthening interfacial polarization produced by charge array orderly in the defects under the applied electric field causes the EV higher than theoretical values.

Furthermore, all those models mentioned above are employed to calculate the dielectric constant of composites. The simulation and experiment values are shown in Fig. 10. According to the results, the predicted ϵ_r values deviate tremendously from the experimental values using Lichtenecker model which is suitable for the composites with similar dielectric constant in two parts. Again, there exists a big deviation of EV and TV using Landzu-Lifshitz model when the content of ceramic is more than 20 vol%. Therefore, it is further proved that this model applies to the composite material containing low content ceramic fillers. Besides, the simulation value and test results of dielectric constant of composites are compared and analyzed, which proved the high accuracy of Yamada and Maxwell models. Particularly, simulation curve obtained by Yamada model with $n=3.2$ is most close to the experimental results.

4 Conclusions

In summary, the effect of different content BST fillers on microstructure and dielectric properties of BST/ABS composites has been performed with a systematic experimental and theoretical investigation. SEM images of composites demonstrated the excellent distribution of BST fillers in ABS matrix. The permittivity and the dielectric tunability of BST/ABS composites increased with increasing the volume fraction of BST fillers. And the dielectric constant of BST/ABS composites decreased with increasing frequency ($10^2 \sim 10^6$ Hz). The dielectric constant and loss tangent increased gradually from room temperature to T_m and exhibited typical dielectric relaxation characteristics. Moreover, the dielectric constants of composites were simulated by using Lichtenecker, Maxwell, Landzu–Lifshitz and Yamada models. Among them, the predicted permittivity

Fig. 9 Theoretical predictions values (TV) and experimental values (EV) of BST/ABS composites in terms of frequency at different volume fractions of BST

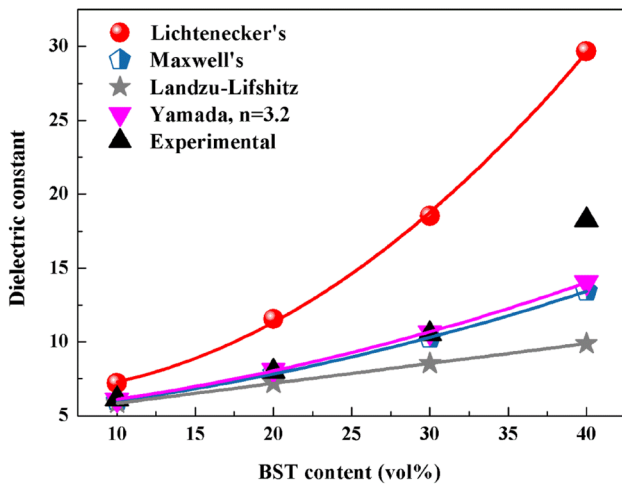
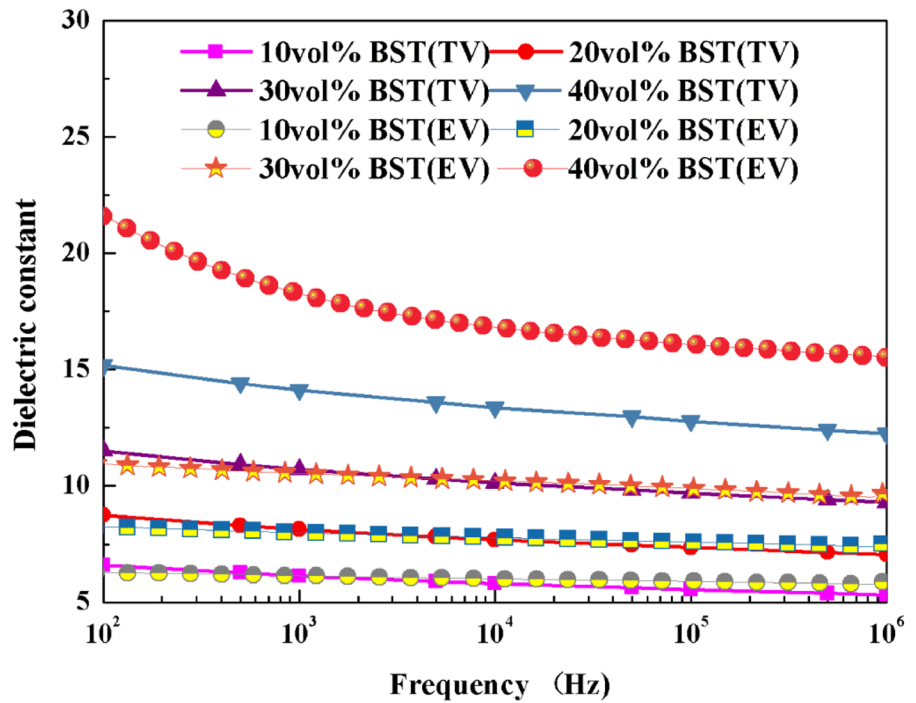


Fig. 10 Experimental and theoretical dielectric constant of BST/ABS composites

of composites by Yamada model exhibited close correspondence to the experimentally determined results, when the shape factor $n=3.2$ was employed. The work of BST/ABS dielectric functional composites developed a suitable functional material for 3D printed electronic devices.

Acknowledgements This work was supported by the National Natural Science Foundation of China (No. 11372249, 51672219), the International Cooperation Foundation of Shanxi Province, the Research Fund of the State Key Laboratory of Solidification Processing (NWPU), China (No.137-QP-2015), and the “111” Project (No. B08040).

References

1. A. Ianculescu, D. Berger, M. Viviani, C.E. Ciomaga, L. Mitoseriu, E. Vasile, N. Dragan, D. Crisan, Investigation of $Ba_{1-x}Sr_xTiO_3$ ceramics prepared from powders synthesized by the modified Pechini route. *J. Eur. Ceram. Soc.* **27**, 3655–3658 (2007)
2. G.X. Hu, F. Gao, L.L. Liu, B. Xu, Z.T. Liu, Microstructure and dielectric properties of highly tunable $Ba_{0.6}Sr_{0.4}TiO_3/MgO/Al_2O_3/ZnO$ composite. *J. Alloy. Compd.* **518**, 44–50 (2012)
3. W.J. Kim, W. Chang, S.B. Qadri, J.M. Pond, S.W. Kirchoefer, D.B. Chrisey, J.S. Horwitz, Microwave properties of tetragonally distorted $(Ba_{0.5}Sr_{0.5})TiO_3$ thin films. *Appl. Phys. Lett.* **76**, 1185–1187 (2000)
4. A. Feteira, D.C. Sinclair, I.M. Reaney, Y. Somiya, M.T. Lanagan, $BaTiO_3$ -based ceramics for tunable microwave applications. *J. Am. Ceram. Soc.* **87**, 1082–1087 (2004)
5. G.X. Hu, F. Gao, L.L. Liu, X. Cao, Z.T. Liu, Microstructure and dielectric properties of $Ba_{0.6}Sr_{0.4}TiO_3-MgAl_2O_4$ composite ceramics. *Ceram. Int.* **37**, 1321–1326 (2011)
6. D. Kim, Y. Choi, M. Ahn, M.G. Allen, P. Marry, 2.4 GHz continuously variable ferroelectric phase shifters using all-pass networks. *IEEE Microw. Wirel. Compon. Lett.* **13**, 434–436 (2003)
7. A. Tombak, J.P. Maria, F. Ayguavives, J. Zhang, G.T. Stauff, A.I. Kingon, A. Mortazawi, Tunable barium strontium titanate thin film capacitors for RF and microwave applications. *IEEE Microw. Wirel. Compon.* **12**, 3–5 (2002)
8. G.X. Hu, F. Gao, J. Kong, S.J. Yang, Q.Q. Zhang, Z.T. Liu, Y. Zhang, H.J. Sun, Preparation and dielectric properties of poly(vinylidene fluoride)/ $Ba_{0.6}Sr_{0.4}TiO_3$ composites. *J. Alloy. Compd.* **619**, 686–692 (2015)
9. W. Chang, L. Sengupta, MgO-mixed $Ba_{0.6}Sr_{0.4}TiO_3$ bulk ceramics and thin films for tunable microwave applications. *J. Appl. Phys.* **92**, 3941–3946 (2002)
10. W. Jo, U.J. Chung, N.M. Hwang, D.Y. Kim, Temperature dependence of the coarsening behavior of $(Ba, Sr)TiO_3$ grains

- dispersed in a SiO₂-rich liquid matrix. *J. Eur. Ceram. Soc.* **23**, 1565–1569 (2003)
11. C. Ang, Z. Yu, R.Y. Guo, A.S. Bhalla, Calculation of dielectric constant and loss of two-phase composites. *J. Appl. Phys.* **93**, 3475–3480 (2003)
 12. N.G. Devaraju, B.I. Lee, Dielectric behavior of three phase polyimide percolative nanocomposites. *J. Appl. Polym. Sci.* **99**, 3018–3022 (2006)
 13. Y. Bai, Z.Y. Cheng, V. Bharti, H.S. Xu, Q.M. Zhang, High-dielectric-constant ceramic-powder polymer composites. *Appl. Phys. Lett.* **76**, 3084–3086 (2000)
 14. L. Ramajo, M. Reboredo, M. Castro, Dielectric response and relaxation phenomena in composites of epoxy resin with BaTiO₃ particles. *Compos Part A* **36**, 1267–1274 (2005)
 15. Z.M. Dang, H.Y. Wang, Y.H. Zhang, J.Q. Qi, Morphology and dielectric property of homogenous BaTiO₃/PVDF nanocomposites prepared via the natural adsorption action of nanosized BaTiO₃. *Macromol. Rapid. Comm.* **26**, 1185–1190 (2005)
 16. C.J. Dias, D.K. Das-Gupta, Inorganic ceramic/polymer ferroelectric composite electrets. *IEEE Trans. Dielectr. Electr. Insul.* **3**, 706–710 (1996)
 17. S.D. Cho, J.Y. Lee, J.G. Hyun, K.W. Paik, Study on epoxy/BaTiO₃ composite embedded capacitor films (ECFs) for organic substrate applications. *Mater. Sci. Eng.* **110**, 233–237 (2004)
 18. Z.M. Dang, Y.F. Yu, H.P. Xu, J. Bai, Study on microstructure and dielectric property of the BaTiO₃/epoxy resin composites. *Compos. Sci. Technol.* **68**, 171–177 (2008)
 19. S.H. Xie, B.K. Zhu, X.Z. Wei, Z.K. Xu, Y.Y. Xu, Polyimide/BaTiO₃ composites with controllable dielectric properties. *Composites Part A* **36**, 1152–1157 (2005)
 20. J.W. Xu, C.P. Wong, Characterization and properties of an organic-inorganic dielectric nanocomposite for embedded decoupling capacitor applications. *Compos Part A* **38**, 13–19 (2007)
 21. Y.Q. Wang, F. Castles, P.S. Grant, 3D printing of NiZn ferrite/ABS magnetic composites for electromagnetic devices. *Mater. Res. Soc. Symp. Proc.* **1788**, 29–35 (2015)
 22. F. Castles, D. Isakov, A. Lui, Q. Lei, C.E.J. Dancer, Y. Wang, J.M. Janurudin, S.C. Speller, C.R.M. Grovenor, P.S. Grant, Microwave dielectric characterization of 3D-printed BaTiO₃/ABS polymer composites. *Sci. Rep.* **6**, 22714 (2016)
 23. Q.Q. Zhang, F. Gao, G.X. Hu, C.C. Zhang, M. Wang, M.J. Qin, L. Wang, Characterization and dielectric properties of modified Ba_{0.6}Sr_{0.4}TiO₃/poly(vinylidene fluoride) composites with high dielectric tenability. *Compos. Sci. Technol.* **118**, 94–100 (2015)
 24. Q.Q. Zhang, F. Gao, C.C. Zhang, L. Wang, M. Wang, M.J. Qin, G.X. Hu, J. Kong, Enhanced dielectric tunability of Ba_{0.6}Sr_{0.4}TiO₃/poly(vinylidene fluoride) composites via interface modification by silane coupling agent. *Compos. Sci. Technol.* **129**, 93–100 (2016)
 25. T. Zhou, J.W. Zha, R.T. Cui, B.H. Fan, J.K. Yuan, Z.M. Dang, Improving dielectric properties of BaTiO₃/ferroelectric polymer composites by employing surface hydroxylated BaTiO₃ nanoparticles. *ACS Appl. Mater. Interfaces* **3**, 2184–2188 (2011)
 26. S. Liu, J. Zhai, J. Wang, S. Xue, W. Zhang, Enhanced energy storage density in poly(vinylidene fluoride) nanocomposites by a small loading of surface-hydroxylated Ba_{0.6}Sr_{0.4}TiO₃ nanofibers. *ACS Appl. Mater. Interfaces* **6**, 1533–1540 (2014)
 27. C.V. Chanmal, J.P. Jog, Dielectric relaxations in PVDF/BaTiO₃ nanocomposites. *Express. Polym. Lett* **2**, 294–301 (2008)
 28. M.Y. Zhao, C.Y. Xu, C.A. Wang, Y. Tang, Relations of (Ba_{1-x}Sr_x)TiO₃ dielectric constant with temperature and frequency. *J. Huazhong Univ. Sci. Technol.* **31**, 72–74 (2003)
 29. H.S. Nalwa *Ferroelectric Polymers: Chemistry, Physics, and Applications*. (CRC Press, Boca Rotan, 1995)
 30. R. Landauer, The electrical resistance of binary metallic mixtures. *J. Appl. Phys* **23**, 779–784 (1952)
 31. B.H. Fan, J.W. Zha, D.R. Wang, J. Zhao, Z.M. Dang, Experimental study and theoretical prediction of dielectric permittivity in BaTiO₃/polyimide nanocomposites films. *Appl. Phys. Lett.* **100**, 09290311–09290314 (2012)
 32. T. Yamada, T. Ueda, T. Kitayama, Piezoelectricity of a high-content lead zirconate titanate/polymer composite. *J. Appl. Phys* **53**, 4328–4332 (1982)